Experimental and Theoretical Investigation of the Reaction of RO₂ Radicals with OH Radicals: Dependence of the HO₂ Yield on the Size of the RO₂ Moiety

Emmanuel Assaf¹, Coralie Schoemaecker¹, Luc Vereecken², Christa Fittschen¹,*

¹Université Lille, CNRS, UMR 8522 - PC2A - Physicochimie des Processus de Combustion et de l'Atmosphère, F-59000 Lille, France

² Institut für Energie und Klimaforschung, Forschungszentrum Jülich GmbH, D-52428 Jülich, Germany

*Corresponding author: Christa Fittschen (christa Fittschen@univ-lille1.fr)

Tel: ++ 33 3 20 33 72 66

Submitted to

International Journal of Chemical Kinetics,

Special issue: ICCK 2017

Abstract

The HO_2 yield in the reaction of peroxy radicals with OH radicals has been determined experimentally by measuring simultaneously OH and HO_2 concentration time profiles, following the photolysis of XeF_2 in the presence of different hydrocarbons and O_2 . The following yields have been obtained: $\phi_{CH3O2} = (0.84\pm0.25)$, $\phi_{C2H5O2} = (0.57\pm0.17)$, $\phi_{C3H7O2} = (0.35\pm0.15)$, $\phi_{C4H9O2} = (0.15\pm0.05)$. The clear decrease in HO_2 yield with increasing size of the alkyl moiety can be explained by an increased stabilization of the trioxide adduct, ROOOH. This has been confirmed by ab-initio and RRKM master equation calculations. It can be expected, that under atmospheric conditions the stabilized adduct, ROOOH, is the only product of the reaction between OH radicals and peroxy radicals containing more than 2 C-atoms. The fate and possible impact of these species is completely unexplored so far.

Introduction

RO₂ radicals play a key role in atmospheric chemistry, and their subsequent reaction pathway can influence the composition of the troposphere. While the major pathway in polluted environments is their reaction with NO, in low NO_x environments the reaction with HO₂ or with other peroxy radicals becomes competitive. It has recently been shown that in clean environments the reaction of peroxy radicals with OH radicals can become competitive and can act as an important sink¹. Indeed, the rate constants for the reaction of CH₃O₂²⁻⁴, C₂H₅O₂⁵ as well as of larger RO₂ radicals⁶ with OH radicals have been measured in recent years and have found to be fast. Models show that on large sections of the globe a nonnegligible fraction of peroxy radicals will decay through this pathway^{1, 7}. Archibald *et al.*⁸ have run different scenarios using a model named BAMBO, based on the MCM mechanism⁹. Different possible reaction paths and rate constants were simulated for the reaction of OH radicals with peroxy radicals up to C4, and unsurprisingly it was found that the nature of the reaction products makes a large difference on the impact of this reaction on the composition of the troposphere. Hence, it is important to investigate the product formation for this class of reactions.

The potential energy surface (PES) for $CH_3O_2 + OH^7$ and $C_2H_5O_2 + OH^{10}$, as well as the reverse $CH_3O + HO_2$ reaction¹¹ proceeding on the same PES,[ref ourselves, others] have been studied in detail using theoretical methodologies. These studies show that the $RO_2 + OH$

reaction proceeds near-exclusively by formation of an ROOOH trioxide intermediate, whose lowest-lying fragmentation channel is formation of RO + HO₂, in agreement with the recent measurements³ of high yields of HO₂ from the CH_3O_2+OH reaction discussed above. Rearrangement of the CH_3O+HO_2 H-bonded complex was predicted to yield methanol + O_2 in minor yields.

$$RO_2 + OH$$
 $\rightarrow ROOOH^*$ \rightarrow $RO -- HO_2$ \rightarrow $RO + HO_2$ (R1a) \rightarrow $ROH + O_2$ (R1b) $\stackrel{M}{\rightarrow}$ $ROOOH$ (thermalized) (R1c)

In a first experimental study¹² on the product yields of the reaction between $CH_3O_2 + OH$, a high yield of 0.8 ± 0.2 for the formation of HO_2 radicals has been found. In this work, we investigate the HO_2 -yield for the three next-large peroxy radicals, $C_2H_5O_2$, $C_3H_7O_2$ and $C_4H_9O_2$. We support the experimental results with a qualitative theoretical analysis of the pressure-dependent yields of the $HO_2 + RO$ products and ROOOH adduct in the $RO_2 + OH$ reaction, as a function of the substrate R.

Experiments

Experimental methodology

The HO_2 yield, Φ_{HO2} , has been obtained from the simultaneous measurement of OH and HO_2 concentration time profiles, using a laser photolysis reactor coupled to two identical cw-CRDS absorption paths, the experimental set-up has been described in detail¹³⁻¹⁵. Briefly, the reaction was initiated by the 248 nm photolysis of XeF_2 in the presence of hydrocarbons RH (methane, ethane, propane or butane) and H_2O , leading to the generation the peroxy radicals and OH radicals through the following reaction sequence:

$$XeF_2 + hv_{248nm} \rightarrow 2 F + Xe \tag{R2}$$

$$RH + F \rightarrow R + HF$$
 (R3)

$$H_2O + F \rightarrow OH + HF$$
 (R4)

$$R + O_2(+M) \rightarrow RO_2 \tag{R5}$$

which is followed by reaction (R1). The reaction product of (R1a), alkoxy radicals, can react in the presence of high O_2 concentrations, leading to an aldehyde and a second HO_2 radicals:

$$RO + O_2 \rightarrow R(.H)O + HO_2 \tag{R6}$$

As for the previous measurement, HO₂ and OH radicals have been quantified by cw-CRDS: HO₂ radicals were detected on one cw-CRDS path¹⁶ at 6638.205 cm⁻¹ and OH radicals¹⁷ were detected simultaneously on the other path at 7028.831 cm⁻¹.

Experiments have been carried out at a total pressure of 50 Torr using three different hydrocarbons: ethane, propane and butane. For each hydrocarbon, experiments have been carried out at two oxygen concentrations, one low concentration at 1.2×10¹⁶ cm⁻³ and one high at 8.0×10^{17} cm⁻³, while keeping other parameters such as photolysis energy and XeF₂ concentration constant by adjusting the concentration of the bath helium gas. Before adding each hydrocarbon, XeF₂ has been photolysed in the presence of only H₂O to estimate the initial concentration of F-atoms, assuming that under these conditions all F atoms will be converted into OH. The difference between the OH concentrations with H₂O only and with H₂O + hydrocarbon can be taken as a good estimation of the concentration of the peroxy radicals. The ratio between initial OH and RO₂ radical concentration is given by the ratio of the rates for (R3) and (R4). The rate constant of F-atoms with H₂O is recommended to $k_4 = 1.4 \times 10^{-11} \text{ cm}^3 \text{s}^{-1}$, while the rate constant for the reaction of F-atoms with different hydrocarbons is not very well known, but is probably several times faster¹⁸ than k₄. Therefore, the hydrocarbon concentration has been adjusted before each experiment such that the remaining OH concentration (and with this the initial RO₂ concentration) was similar for each hydrocarbon. The initial radical concentrations obtained for OH and RO₂ in presence of hydrocarbon were around 1.6×10^{12} cm⁻³ and between 5 - 6×10^{12} cm⁻³ respectively, with ratios of RO₂/OH around 3 to 4. The conditions and results of all experiments are summarized in Table 1.

Experimental results

The reaction of F-atoms with propane and butane can lead to the formation of both 1-and 2-propyl / butyl radicals. However, the yields of the different isomers are not well known, and in the frame of this work we do not make a distinction between the two isomers. The **Figure 2** presents the concentration time profiles of OH (left) and HO₂ (right), obtained

during the experiments presented in **Table 1**. The experiments with CH₄ are not shown; no experiments can be carried out with low O₂ concentrations, as (R5) is too slow to convert CH₃ fast enough into CH₃O₂. The black dots in **Figure 2** show the OH concentrations, obtained in the absence of any hydrocarbon and can be seen as an estimation of the total radical concentration (experiments A in Table 1). No HO₂ was observed under these conditions. It can be seen that the OH radical decays are on the same timescale as the increase of the HO₂ concentration, in line with the assumptions that HO₂ radicals are a direct product of (R1) under low O₂ concentrations (experiments B in **Table 1**) and that their formation is not the rate limiting step under high O₂ concentrations (experiments C in **Table 1**). The blue dots represent the experiments carried out under low O₂ concentrations (1.2×10¹⁶ cm⁻³): under these conditions, the formation of RO_2 radicals is fast for all alkyl radicals (k5' $\approx 1\times10^5$ s⁻¹) except for CH₃. The subsequent reaction of the corresponding alkoxy radicals (R6) is still slow on our time scale for ethoxy, 1- and 2-propoxy¹⁹ and 2-butoxy²⁰ (k_6 ' $\approx 130s^{-1}$) while the 1-butoxy radical is believed to undergo rapid intramolecular isomerization 21 . At the high O_2 concentration experiments (8×10¹⁷ cm⁻³), k_6 becomes fast enough (k_6 ' ≈ 8000 s⁻¹) to convert RO radicals within 100µs into aldehyde and HO₂, only the isomerization of the 1-butoxy radical will probably be still faster than its reaction with O_2 .

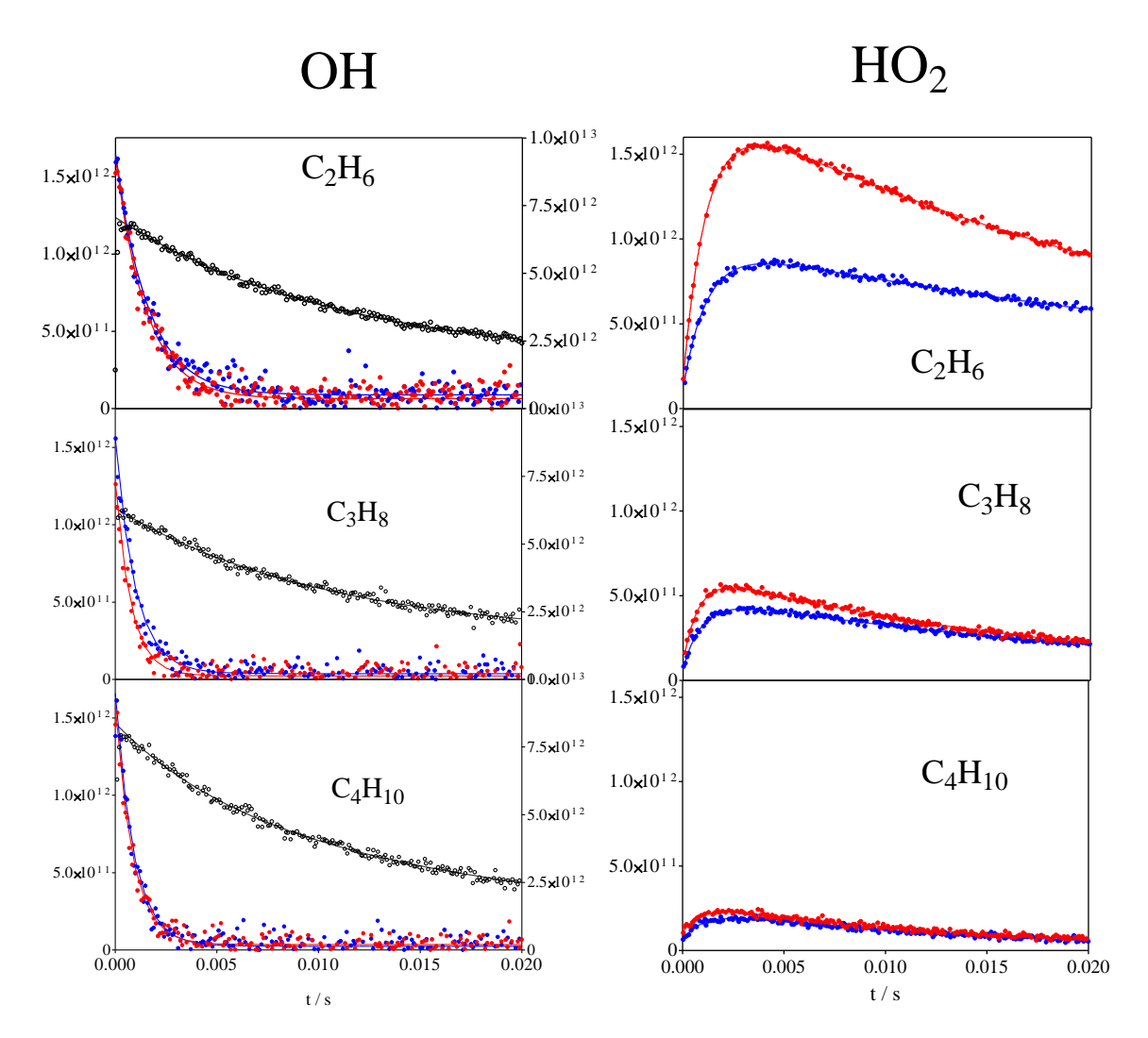


Figure 2: OH concentration time profiles for all experimental conditions given in **Table 1** (except for CH_4). The black symbols show the OH concentrations in the absence of hydrocarbons (experiments 1 in Table 1), and are representative for the total radical concentration (right y-axis), the blue and red symbols show the OH profile in the presence of hydrocarbons and low (experiments B in Table 1) and high (experiments C in Table 1) O_2 concentrations (left y-axis)

The graphs for all three radicals are at the same scale, and it can be seen immediately that the HO_2 yield strongly decreases with increasing size of the hydrocarbon. The decay rate of the OH radical is not influenced by the O_2 -concentration. In a first approximation, the HO_2 concentration-time profiles have been fitted to an association-dissociation fit (full lines in **Figure 2**), *i.e.* assuming a pseudo-first order formation and consumption of HO_2 radicals

$$[HO_2] = [HO_2]_{ini} \times e^{-k_{slow}t} + [HO_2]_{sec} \times \frac{k_{fast}}{k_{slow} - k_{fast}} (e^{-k_{fast}t} - e^{-k_{slow}t})$$
 [Eq. 2]

The fit –parameters of all seven HO₂ profiles (CH₄ not shown in **Figure 2**), together with the results from a fit to a mono-exponential decay of the corresponding OH decay curves, are presented in **Table 1**:

Table 1: Experimental conditions and fit parameters from **Figure 2** for all experiments. Hydrocarbon concentrations were [HC] = 0 cm⁻³ for all experiments A, for B and C as follows: Exp. 1:[CH₄] = 4.6×10^{14} cm⁻³; Exp. 2: [C₂H₆] = 2.1×10^{14} cm⁻³, Exp. 3: [C₃H₈] = 2.6×10^{14} cm⁻³, Exp. 4: [C₄H₁₀] = 1.2×10^{14} cm⁻³, [O₂] = 1.2×10^{16} cm⁻³ for all experiments A and B, and [O₂] = 8×10^{17} cm⁻³ for all experiments C.

Exp. No.	[OH] ₀ / 10 ¹² cm ⁻³	$[RO_2]^a / 10^{12} \text{ cm}^{-3}$	k' _{OH} / s ⁻¹	% OH ^b with RO ₂	k _{OH+RO2} / 10 ⁻¹⁰ cm ³ s ⁻¹	[HO ₂] _{ini} / 10 ¹⁰ cm ⁻³	% [HO ₂] _{ini} ^d	[HO ₂] _{sec} / 10 ¹¹ cm ⁻³	k _{fast} / s	$\Phi_{ ext{HO2}}^{}e}$
1A	6.02	0								
1C	1.59	1.18	575	79	1.0	5.07	1.13	1.98	622	1.67
2A	7.06	0	91	-						
2B	1.56	5.5	669	79	9.7	12.5	2.3	8.37	861	0.57
2C	1.56	5.5	630	78	9.0	17.7	3.2	16.0	870	1.18
3A	6.33	0	95	-						
3B	1.52	4.8	1011	65	1.4	6.9	1.4	4.20	1045	0.35
3C	1.25	5.1	1282	73	1.8	10.1	2.0	5.22	1340	0.46
4A	8.10	6.50	92	-						
4B	1.64	6.66.5	1090	70	1.2	6.1	1.0	1.70	1026	0.15
4C	1.53	6.6	1147	71	1.2	10.6	1.6	1.66	1175	0.15

 $^{^{}a} \ [RO_{2}] \ calculated \ from \ ([OH]_{0,without \ alkane} - [OH]_{0 \ with \ alkane})$

The rapid HO_2 (named $[HO_2]_{sec}$) can be, under low O_2 concentrations, associated with the HO_2 formed in reaction (R1a), while at high O_2 concentrations it corresponds to the sum of the HO_2 formed in (R1a) and (R6). $[HO_2]_{ini}$ is a small HO_2 concentration that forms immediately on our time scale and is thought to be formed in the reaction of hot alkyl radicals with O_2 . This hypothesis is in line with the observation that the yield of $[HO_2]_{ini}$, obtained from the fitted value divided by the initial RO_2 concentration (a) decreases with increasing size of the alkyl radicals (except for CH_4) and (b) increases with increases O_2 concentration.

^b % OH having reacted with RO₂, calculated from (k'_{OH} – k'_{HC}-k'_{OH without alkane}) / k'_{OH} × 100

^c Rate constant of (R1) obtained from (k'_{OH} – k'_{HC}-k'_{OH without alkane}) / [RO₂]

 $^{^{}d}$ % [HO₂]_{ini} calculated from [HO₂]_{ini} / [RO₂] × 100

^e φ_{HO2} calculated from [HO₂]_{sec} / [OH] having reacted with RO₂

The yield of HO_2 radicals in (R1) has then been calculated as the concentration of $[HO_2]_{sec}$ radicals, formed under low O_2 conditions, divided by the concentration of OH radicals having reacted with RO_2 radicals. The following yields have been obtained (last column in **Table 1**): $\Phi_{HO2} = 0.57 \pm 0.17$, $\Phi_{HO2} = 0.35 \pm 0.15$ and $\Phi_{HO2} = 0.15 \pm 0.05$ for $C_2H_5O_2$, $C_3H_7O_2$ and $C_4H_9O_2$, respectively The error bars have been estimated to \pm 30%, with the most important error sources being (a) the XeF_2 concentration that might fluctuate between experiments A and B, and (b) the reliability of the OH and HO_2 absorption signals: errors in the absolute values of the absorption cross sections will be negligible, as both cross sections have been determined together in our set-up¹⁷, and thus errors would cancel out to a large extend. However, both absorption features, OH and HO_2 , have sharp absorption lines, so a small deviation of the laser wavelengths will lead to a change in absorption signal.

The HO_2 yield for the experiments with higher O_2 concentrations is expected to be twice as high for C_2H_6 and C_3H_8 , because no other fate then (R6) is expected for these two alkoxy radicals. Indeed, the value for CH4 obtained in the frame of this work ($\Phi_{HO2} = 1.67 / 2 = 0.84$) is in excellent agreement with our recent determination 12. For C_2H_6 , the results are in perfect agreement with these expectations (0.57 and 1.18) at low and high O_2 , while this is not the case anymore for the propane: at high O_2 concentrations, some HO_2 is "missing" at high O_2 : 0.35 and 0.46. For butane, the HO_2 yield at high O_2 is even identical to the yield at low O_2 : this is anticipated because of a fast intramolecular isomerisation of n-butoxy instead of reacting with O_2^{21} . However, it can be assumed that the reaction of F-atoms with n-butane leads also to the formation of 2-butylradicals, in which case the 2-butoxy radical would be formed and some increase in HO_2 yield was expected to be observed. No conclusive explanation can be given to these unexpected low HO_2 yields, further experiments will be carried out in the future to elucidate this question.

Finally, the rate constant of the reaction of OH-radicals with all four RO_2 radicals has been estimated from these experiments: the OH decay rate (after subtraction of the decay due to reaction with the hydrocarbon minus the OH decay in absence of hydrocarbon) has been divided by the concentration of RO_2 radicals: rate constants of $k_1 = (0.9 - 1.8) \times 10^{-10}$ cm³s⁻¹ have been obtained for the different radicals and O_2 concentrations. These values have large error bars, given the only rough estimation of the RO_2 radical concentration However, the good overall agreement with earlier, more direct determinations^{3, 5-6} can be taken as an indicator that the assumptions made for deducing the HO_2 yields are valid.

Theory

Theoretical methodology

The accurate characterization of the potential energy surface of the RO₂ + OH reaction is highly demanding, as both the main entrance and exit channels are barrierless; this requires a characterization of the entire reaction channel and a variational optimization of the kinetic transition state. Furthermore, as documented extensively by Müller et al.⁷, the energy profile and rovibrational characteristics of these channels are very sensitive to the level of theory employed, making such computations expensive and less reliable. Secondly, the rate of collisional stabilization of the ROOOH trioxide intermediate is likewise hard to describe, as the predicted energy transfer in collisions with the bath gas depends strongly on the values of the parameters used in the collision model; these values typically carry a large uncertainty. Given the computational expense of generating reliable absolute rate coefficients for all the competing processes, it was chosen to instead build a qualitative model representing the main features of the reaction class, but aim only for a semi-quantitative analysis of the reactivity trends. In such a model, the competition between the reaction across the barrierless channels and collisional energy loss is then optimized by calibration against experimental data. In this work, we will use the experimental results on the C₂H₅O₂+OH reaction as our reference, tuning the entropy of the kinetic bottleneck in the barrierless channels to reproduce the observed HO₂ yield. The remaining alkylperoxy radicals, CH₃O₂, n-C₃H₇O₂, and n-C₄H₉O₂, are then treated identically, without further tuning as described below, yielding an estimate of the HO₂ yields and ROOOH stabilization relative to the ethylperoxy reference reaction as governed by the quantum chemical trends in rovibrational characteristics across these compounds.

The geometries and rovibrational characteristics of the critical points on the PES are optimized at the M06-2X/aug-cc-pVTZ level of theory²²⁻²³; the relative energies are further refined at the CCSD(T)/aug-cc-pVTZ level of theory²³⁻²⁵. All calculations were performed using Gaussian-09²⁶. As we focus here on the yields of the main products, we chose to simplify the potential energy somewhat, neglecting all minor channels that are unable to compete effectively against the energetically and entropically most favorable barrierless channels. We thus omit all reactions on the triplet surface, owing to their distinct energy barriers^{7, 10-11} of several kcal mol⁻¹. Likewise, the H-abstraction reaction on the singlet

surface, making carbonyl oxides (>C=O $^+$ -O $^-$ compounds, also known as Criegee intermediates) + H₂O do not contribute, with calculated rate coefficients of the order of $1\times10^-$ 13 cm³s⁻¹ (R=CH₃) and 7×10^{-13} cm³s⁻¹ (R=C₂H₅). Finally, several fragmentation channels exist^{7, 10-11} for the ROOOH trioxide intermediate, but except for the RO+HO₂ products, these all have high energy barriers and do not contribute significantly. As discussed extensively by Müller et al.⁷ and by Assaf et al.¹¹, the RO + HO₂ fragments can form an H-bonded complex RO--HO₂, which can fall apart to the free products, re-arrange to ROH + O₂. This secondary chemistry does not affect the alkyl-dependence of the initial steps, and is outside the scope of our current relative product yield study.

The PES is thus reduced to the main channels as depicted in Figure 1, i.e. formation of the ROOOH adduct, where the nascent, chemically activated adducts either re-dissociate to the reactants, dissociate to $RO + HO_2$, or get stabilized by collisional energy loss.

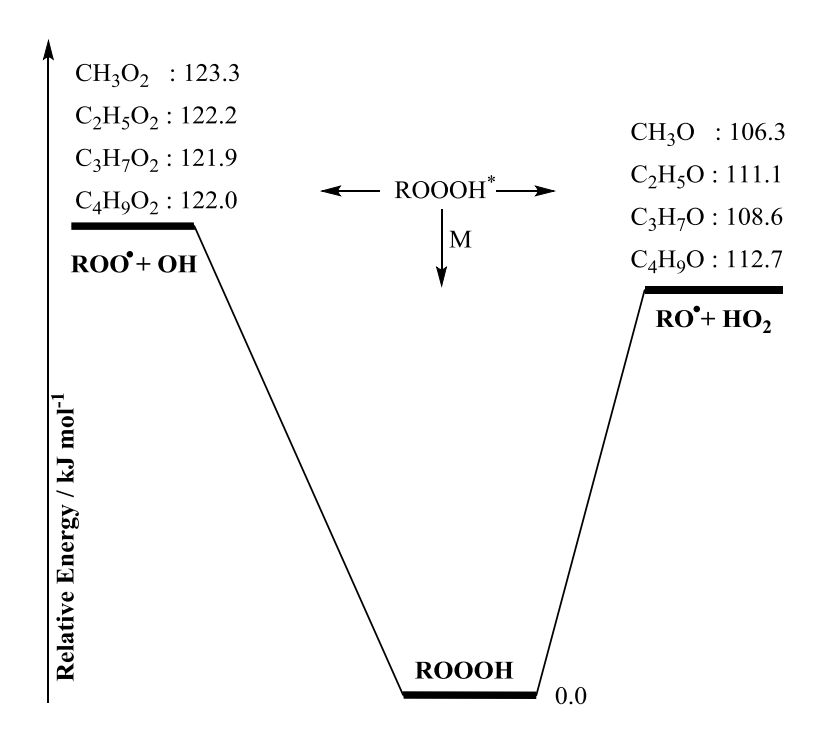


Figure 1: Simplified potential energy surface of the RO_2 + OH reaction at the CCSD(T)/aug-cc-pVTZ//M06-2X/aug-cc-pVTZ level of theory, for $R = CH_3$, C_2H_5 , $n-C_3H_7$ and $n-C_4H_9$. The main channels accessible to the nascent, energy-rich $ROOOH^*$ adduct is redissociation to the reactants, dissociation to $RO + HO_2$, or thermalization in collisions with the bath gas.

The product distribution for all reaction studied is then obtained by master equation analysis of the mechanism, based on RRKM rate coefficients. The master equations are solved using the CSSPI method, and was verified using the DCPD solution method²⁷, both of

which build on a matrix formulation of the underlying Monte Carlo random walk of the energized adduct Collisional energy loss in the nascent, chemically activated ROOOH* intermediates is modeled in RRKM-based master equation calculations, using the Troe biexponential collisional energy transfer model²⁸ with for all ROOOH an average energy transfer of $\Delta E_{ave} = 3.75 \text{ kJ mol}^{-1}$ in N₂ bath gas, mimicking the value used by Müller et al.⁷ for consistency, and $\Delta E_{ave} = 2.1 \text{ kJ mol}^{-1}$ in He. Lennard-Jones collisional parameters used are $\varepsilon_{A-A}=350$ K for all ROOOH, and $\sigma_{A-A}=5.4, 5.8, 5.9,$ and 6.2 Å for CH₃OOOH, C₂H₅OOOH, n-C₃H₇OOOH, and n-C₄H₉OOOH, respectively. Bath gas is air, at a pressure of 1 atm. The rovibrational characteristics of the kinetic bottleneck of all barrierless channels are obtained from a single structure on the minimum energy path, obtained by constrained geometry optimizations at an arbitrarily chosen ROO-OH distance, identical for all reactions. The energy of the chosen critical point is set to the reactant/product. As a means for calibration, a scaling factor S is introduced that scales the wavenumbers of the transitional modes. These modes have the strongest influence on the energy-specific rate coefficient of the reactions, whereas the conserved modes typically vary only moderately across the reaction path. S is optimized such that the predicted HO₂ yield in the C₂H₅O₂+OH reaction matches the experimentally obtained product yield. The same factor S is applied to all barrierless reactions, for all alkyl groups considered, and is the only tunable parameter in our analysis. This qualitative methodology does not yield reliable absolute rate coefficient, but is expected to give reasonable ratio k_{uni}/k_{collision} for energy-specific unimolecular reaction rate coefficient for ROOOH* versus its multi-step collisional stabilisation to ROOOH.

Theoretical analysis

As shown in **Figure 1**, the potential energy surface for $RO_2 + OH \rightarrow ROOOH \rightarrow RO+HO_2$ reaction sequence is largely independent of the alkyl group in the reactants, where we find that the exit channel to $RO + HO_2$ lies on average 12.7 kJ mol⁻¹ below the $RO_2 + OH$ entrance channel. This concurs with the calculations available in the literature data for methyl and ethyl peroxy radicals^{7, 10-11}. In all cases, the exothermic product channel allows for direct dissociation of chemically activated ROOOH adducts. The collision number, and stabilization rates remain comparable across all ROOOH adducts considered. However, the excess energy available to the trioxide adduct is distributed across all degrees of freedom, the number of which increase significantly for larger R-substrates. This slows down the rate of dissociation

such that the competition of collisional energy loss becomes more important as the R-group becomes larger.

Table 2 and **Table 3** list the results of the RRKM master equation calculations for all RO₂ radicals considered. As expected, redissociation of the trioxide adduct to the reactants is negligible in all cases. In the experimental conditions of 50 Torr He (see Table 2), fragmentation to RO + HO₂ is by far the dominant path for small alkyl groups; the nearcomplete conversion to CH₃O + HO₂ in the CH₃O₂ + OH reaction is in agreement with earlier experimental¹² and theoretical work⁷. For larger alkyl groups, we see that collisional stabilization of the ROOOH increases in importance, and for alkyl-groups larger than C₄H₉, it is expected that the yield of HO₂ becomes very minor. While the absolute values in **Table 2** rely on the calibration of the theoretical predictions to the experimental HO₂ yield in the C₂H₅O₂ + OH reaction, the predicted trend as a function of the R-substrate relative to this reference reaction is solely the result of the changing molecular properties as derived from the quantum chemical predictions. The good agreement, within the expected uncertainty, of the predicted HO₂ yields compared to the experimental results in this paper across all Rgroups considered, thus supports the experimental observations, and indicates that the product yield trends are mostly due to changes in the fragmentation rate of the ROOOH intermediate.

In the atmosphere, at a higher pressure of 1 atm. and with the more efficient N_2 or O_2 colliders (see **Table 3**), we predict an increased yield of stabilized ROOOH. While fragmentation to $CH_3O + HO_2$ remains the dominant product channel in the CH_3O_2+OH reaction, peroxy radicals with 2 or more carbons are predicted to undergo mostly collisional stabilisation of the trioxide intermediate. In these conditions, kinetic models will have to incorporate the secondary chemistry of the trioxide to express the impact of the title reactions. The predictions at 1 atm. still benefit from our calibration of the ratio of dissociation to collisional stabilization for the $C_2H_5O_2 + OH$ reaction in lower-pressure conditions, as changing the bath gas is equivalent to a relative rate increase, which is more reliable than *a priori* absolute estimates. Still, the predictions are still expected to carry a sizable uncertainty which can be as high as a factor of 1.5 on the product yields.

Table 2: Product yields of the RO₂+OH reactions at 298K and 50 Torr He, as a function of the alkyl group R.

Alkyl group R	Redissociation to RO ₂	Fragmentation to	Stabilisation of	
	+ OH	$RO + HO_2$	ROOOH	
CH ₃	1.5 %	98 %	0.004 %	
C_2H_5	2.2 %	(57 %) ^a	40 %	
$n-C_3H_7$	0.7 %	17 %	81 %	
n-C ₄ H ₉	1.6 %	4 %	96 %	

^a Calibrated approximately against the experimental HO₂ yield.

Table 3: Product yields of the RO₂+OH reactions at 298K and 1 atm N₂, as a function of the alkyl group R.

Alkyl group R	Redissociation to RO ₂	Fragmentation to	Stabilisation of
	+ OH	$RO + HO_2$	ROOOH
CH ₃	1.2 %	91 %	8 %
C_2H_5	0.5 %	11 %	89 %
$n-C_3H_7$	0.08 %	1.5 %	98 %
n-C ₄ H ₉	0.01 %	0.3 %	99.7 %

Conclusions

The HO₂ yields for the reaction of RO₂ radicals with OH radicals has been determined experimentally for 4 differently sized peroxy radicals. Radicals have been generated from the reaction of F-atoms with the corresponding hydrocarbons, in the presence of O₂. The HO₂ yield obtained experimentally are: $\phi_{\text{CH3O2}} = (0.84 \pm 0.25)$, $\phi_{\text{C2H5O2}} = (0.57 \pm 0.17)$, $\phi_{\text{C3H7O2}} = (0.35 \pm 0.15)$, $\phi_{\text{C4H9O2}} = (0.15 \pm 0.05)$.

The experimental results are supported semi-quantitatively by RRKM master equation calculations on a simplified potential energy surface. A single adjustable parameter is used to calibrate the absolute HO_2 yield in the $C_2H_5O_2+OH$ reaction; the analysis then correctly recovers the product yield trends across all four alkyl groups studied. The mechanism behind the reducing HO_2 yield for larger R-groups is thus confirmed to be due to increasing importance of stabilization of the ROOOH intermediate; for substrates larger than $R = C_4H_9$, a negligible HO_2 yield is predicted, with near 100% yields of the trioxide intermediate. The smallest peroxy radical, CH_3O_2 , on the other hand, will not form a sizable fraction of stabilized trioxide. At atmospheric pressures, the formation of stabilized trioxide become the dominant channel for all peroxy radicals except CH_3O_2 ; for this latter the formation of HO_2 is still the major path.

The fate of the thermalized ROOOH adduct was discussed earlier by Müller et al.;⁷ these authors considered thermal decomposition, reaction with atmospheric oxidants such as OH, hydrolysation reactions, and uptake to the aqueous phase. The relative importance of these sinks likely depends on temperature, relative humidity, and other factor.

Acknowledgements

This project was supported by the French ANR agency under contract No. ANR-11-LabEx-0005-01 CaPPA (Chemical and Physical Properties of the Atmosphere), the Région Hauts-de-France, the Ministère de l'Enseignement Supérieur et de la Recherche (CPER Climibio) and the European Fund for Regional Economic Development.

References

- 1. Fittschen, C.; Whalley, L. K.; Heard, D. E. The Reaction of CH₃O₂ Radicals with OH Radicals: A Neglected Sink for CH₃O₂ in the Remote Atmosphere. *Environ. Sci. Technol.* **2014**, *118*, 7700–7701
- 2. Bossolasco, A.; Faragó, E. P.; Schoemaecker, C.; Fittschen, C. Rate Constant of the Reaction between CH₃O₂ and OH Radicals. *Chem. Phys. Lett.* **2014**, *593*, 7-13
- 3. Assaf, E.; Song, B.; Tomas, A.; Schoemaecker, C.; Fittschen, C. Rate Constant of the Reaction between CH₃O₂ Radicals and OH Radicals revisited. *J. Phys. Chem. A* **2016**, *120*, 8923-8932
- 4. Yan, C.; Kocevska, S.; Krasnoperov, L. N. Kinetics of the Reaction of CH₃O₂ Radicals With OH Studied Over the 292 526 K Temperature Range. *J. Phys. Chem. A* **2016**, *120*, 6111–6121
- 5. Faragó, E. P.; Schoemaecker, C.; Viskolcz, B.; Fittschen, C. Experimental Determination of the Rate Constant of the Reaction between $C_2H_5O_2$ and OH Radicals. *Chem. Phys. Lett.* **2015**, *619*, 196-200
- 6. Assaf, E.; Tanaka, S.; Kajii, Y.; Schoemaecker, C.; Fittschen, C. Rate constants of the reaction of C₂–C₄ peroxy radicals with OH radicals. *Chem. Phys. Lett.* **2017**, *684*, 245-249
- 7. Müller, J.-F.; Liu, Z.; Nguyen, V. S.; Stavrakou, T.; Harvey, J. N.; Peeters, J. The Reaction of Methyl Peroxy and Hydroxyl Radicals as a Major Source of Atmospheric Methanol. *Nature Communications* **2016**, *7*, 13213
- 8. Archibald, A. T.; Petit, A. S.; Percival, C. J.; Harvey, J. N.; Shallcross, D. E. On the Importance of the Reaction between OH and RO₂ Radicals. *Atmos. Sci. Lett.* **2009**, *10*, 102-108
- 9. Saunders, S. M.; Jenkin, M. E.; Derwent, R. G.; Pilling, M. J. Protocol for the Development of the Master Chemical Mechanism, MCM v3 (Part A): Tropospheric Degradation of Non-Aromatic Volatile Organic Compounds. *Atmos. Chem. Phys.* **2003**, *3*, 161-180

- 10. Liu, Y.; Chen, L.; Chen, D.; Wang, W.; Liu, F.; Wang, W. Computational study on mechanisms of C₂H₅O₂+OH reaction and properties of C₂H₅O₃H complex. *Chemical Research in Chinese Universities* **2017**, *33*, 623-630
- 11. Assaf, E.; Schoemaecker, C.; Vereecken, L.; Fittschen, C. The reaction of fluorine atoms with methanol: yield of CH3O/CH2OH and rate constant of the reactions CH3O + CH3O and CH3O + HO2. *PCCP* **2018**,
- 12. Assaf, E.; Sheps, L.; Whalley, L.; Heard, D.; Tomas, A.; Schoemaecker, C.; Fittschen, C. The Reaction between CH₃O₂ and OH Radicals: Product Yields and Atmospheric Implications. *Environ. Sci. Technol.* **2017**, *51*, 2170-2177
- 13. Votava, O.; Masat, M.; Parker, A. E.; Jain, C.; Fittschen, C. Microcontroller Based Resonance Tracking unit for Time Resolved Continuous wave Cavity-Ringdown Spectroscopy Measurements. *Rev. Sci. Instrum.* **2012**, *83*, 043110
- 14. Parker, A.; Jain, C.; Schoemaecker, C.; Szriftgiser, P.; Votava, O.; Fittschen, C. Simultaneous, Time-Resolved Measurements of OH and HO₂ Radicals by Coupling of High Repetition Rate LIF and cw-CRDS Techniques to a Laser Photolysis Reactor and its Application to the Photolysis of H₂O₂ *Appl. Phys. B* **2011**, *103*, 725-733
- 15. Faragó, E. P.; Viskolcz, B.; Schoemaecker, C.; Fittschen, C. Absorption Spectrum and Absolute Absorption Cross Sections of CH₃O₂ Radicals and CH₃I Molecules in the Wavelength Range 7473–7497 cm⁻¹. *J. Phys. Chem. A* **2013**, *117*, 12802-12811
- 16. Thiebaud, J.; Crunaire, S.; Fittschen, C. Measurement of Line Strengths in the 2ν₁ Band of the HO₂ Radical using Laser Photolysis / Continous wave Cavity Ring Down Spectroscopy (cw-CRDS). *J. Phys. Chem. A* **2007**, *111*, 6959-6966
- 17. Assaf, E.; Fittschen, C. Cross Section of OH Radical Overtone Transition near 7028 cm⁻¹ and Measurement of the Rate Constant of the Reaction of OH with HO₂ Radicals. *J. Phys. Chem. A* **2016**, *120*, 7051-7059
- 18. Atkinson, R.; Baulch, D. L.; Cox, R. A.; Crowley, J. N.; Hampson, R. F.; Hynes, R. G.; Jenkin, M. E.; M. J. Rossi; Troe, J. Evaluated Kinetic and Photochemical Data for Atmospheric Chemistry: Volume II Gas Phase Reactions of Organic Species. *Atmos. Chem. Phys.* **2006**, *6*, 3625-4055
- 19. Fittschen, C.; Frenzel, A.; Imrik, K.; Devolder, P. Rate Constants for the Reactions of C_2H_5O , i- C_3H_7O , and n- C_3H_7O with NO and O_2 as a Function of Temperature. *Int. J. Chem. Kinet.* **1999**, *31*, 860-866
- 20. Falgayrac, G.; Caralp, F.; Sokolowski-Gomez, N.; Devolder, P.; Fittschen, C. Rate Constants for the Decomposition of 2-Butoxy Radicals and their Reaction with NO and O₂. *Phys. Chem. Phys.* **2004**, *6*, 4127-4132
- 21. Lendvay, G.; Viskolcz, B. Ab Initio Studies of the Isomerization and Decomposition Reactions of the 1-Butoxy Radical. *J. Phys. Chem. A.* **1998**, *102*, 10777-10786
- 22. Zhao, Y.; Truhlar, D. G. The M06 Suite of Density Functionals for Main Group Thermochemistry, Thermochemical Kinetics, Noncovalent Interactions, Excited States, and Transition Elements: Two new Functionals and Systematic Testing of four M06-class Functionals and 12 other Functionals. *Theor. Chem. Acc.* **2008**, *120*, 215-241
- 23. Dunning, T. H. Gaussian Basis Sets for Use in Correlated Molecular Calculations. I. The Atoms Boron through Neon and Hydrogen. *J. Chem. Phys.* **1989**, *90*, 1007-1023
- 24. Purvis, G. D.; Bartlett, R. J. A full coupled-cluster singles and doubles model: The inclusion of disconnected triples. *J. Chem. Phys.* **1982**, *76*, 1910
- 25. Rittby, M.; Bartlett, R. J. An open-shell spin-restricted coupled cluster method: application to ionization potentials in nitrogen. *J. Phys. Chem.* **1988**, *92*, 3033-3036
- 26. Frisch, M. J.; Trucks, G. W.; Schlegel, H. B.; Scuseria, G. E.; Robb, M. A.; Cheeseman, J. R.; Scalmani, G.; Barone, V.; Mennucci, B.; Petersson, G. A., *et al.* Gaussian 09, Revisition B.01. *Gaussian Inc.*, *Wallington CT* **2010**,

- 27. Vereecken, L.; Huyberechts, G.; Peeters, J. Stochastic simulation of chemically activated unimolecular reactions. *J. Chem. Phys.* **1997**, *106*, 6564
- 28. Troe, J. Theory of Thermal Unimolecular Reactions at Low-Pressures. *J. Chem. Phys.* **1977**, *66*, 4745